HEFAT2014
10th International Conference on Heat Transfer, Fluid Mechanics and Thermodynamics
14 – 26 July 2014
Orlando, Florida

TEMPERATURE DISTRIBUTION PROFILES INSIDE BIOMASS UNDER DIELECTRIC BREAKDOWN CONDITIONS

Munoz-Hernandez A., Sharma N., Diaz G.*
*Author for correspondence
School of Engineering
University of California, Merced
5200 N. Lake Rd
Merced, CA, USA
E-mail: gdiaz@ucmerced.edu

ABSTRACT

Under the effect of a sufficiently strong electric field, all materials suffer from a form of breakdown, which involves the flow of current through them. Although wood is sometimes utilized as an electrical insulator, it is also subject to breakdown when exposed to high electric fields. In general, dielectric breakdown is considered a negative effect for electrically insulating materials since it implies the loss of insulating properties of the material. However, the high temperatures generated inside the material can be used as an efficient way to induce the thermo-chemical decomposition of biomass with the purpose of sustainable energy generation. A mathematical model of the dynamics of temperature and electric field inside a small piece of biomass is developed to study temperature distribution and thermal instability growth under thermal dielectric breakdown conditions. A two-dimensional model is implemented for different electric field strengths with biomass dielectric properties obtained from the literature. Temperature, current and electric potential distributions have been analyzed and reported for several cases. The temperature development over time has also been analyzed and reported. The results show that higher voltages lead to almost instantaneous thermal breakdown. Similar results are obtained for AC voltage when the frequency is decreased. These conditions are desired for efficient gasification of biomass.

INTRODUCTION

Biomass gasification has a great potential for sustainable energy generation [1-3]. The process of biomass gasification is used to generate syngas, a mixture rich in H_2 and CO. Syngas can be used in gas turbines to generate electricity or in other applications that require heating from direct combustion of the syngas. Biomass is readily available from tree trimmings in each city, town, etc., nearby forests after logging or clearance for construction of roads etc., and agricultural waste for example. Instead of throwing these trimmings away in the landfills, or burning the left over trimmings or agricultural wastes, these byproducts can be efficiently gasified producing syngas for later usage, thus, reducing the production of CO_2 and/or reducing the amount of waste in landfills and extracting energy from an otherwise undesired byproduct. Though most of the current gasification processes involve conventional downdraft gasifiers [1] and plasma assisted gasifiers [2,3], we introduce a novel idea of gasification through the use of dielectric breakdown, which is deeply discussed next.

Dielectric breakdown of solid materials has been studied extensively since the early 1900's [4-9]. Breakdown can be analyzed as pure electric or thermal [4]. Several theories and specific cases exist to study both types of breakdown. Studies suggest that breakdown in solid dielectrics is set forth by the instabilities created by the localized rise in temperature due to high electrical conduction and Joule heating [5,6]. When excess heat is generated inside the dielectric and the heat is not dissipated at the same rate or faster, the temperature starts rising very rapidly. Most of the electrical and physical properties of wood are dependent on temperature; however, electrical conductivity has a much stronger dependence on it. Due to this fact, once the temperature starts increasing, so does the electrical conductivity and this inter-relation causes a closed loop in which both the temperature and the electrical conductivity increase very rapidly until thermal breakdown occurs.

Nagao et al. investigated the effect of localized temperature rise in the breakdown of polyethylene films [6]. Their results suggested that the breakdown process is dependent on the local increase in temperature, and, additionally, on local weak points of the films.

O'Dwyer presented a review of the latest theories of dielectric breakdown in solids [4]. He mentioned that dielectric breakdown can be analysed as thermal or electric, and electric breakdown can be further subdivided into two different

categories, intrinsic and avalanche. Thermal breakdown can be derived from the basic energy equation [4]:

$$C_v \frac{dT}{dt} - \nabla \cdot (k \nabla T) = \gamma E^2 \quad (1)$$

where C_v is the heat capacity per unit volume, k is the thermal conductivity, T is temperature, γ is electrical conductivity, and E is the electric field, which is dependent on temperature and, therefore, solved for simultaneously. Semi-empirical correlations for the exponential dependence of the electrical conductivity on electric field and temperature were discussed.

The energy equation (1) can be simplified and solved analytically for steady-state, transient, isothermal solid, or it can be solved in full form by employing numerical methods [7]. Because the electrical conductivity has a much stronger dependence on temperature compared to the rest of the physical properties, in the study of thermal breakdown it is often assumed that the remaining properties remain constant and only the change in electrical conductivity is accounted for in the analysis.

Frölich developed his theory of dielectric breakdown to account for the thermal instabilities at high temperatures [8]. He showed that the dielectric breakdown strength above a critical temperature T_c decreases with operating temperature. He noted that these findings differed from other theories which suggested that if the operating temperature is lower than a critical temperature T_c, the dielectric breakdown strength increased with increasing temperature. He argued that each theory is valid only for temperatures above or below a critical temeperature T_c, which is dependent on material properties.

Sze analyzed the behavior of the current transport on silicon nitride films and the maximum dielectric strength [9]. He found that at a set electric field and temperature the current does not depend on the material thickness, bulk properties or polarity. They determined that current transport has three main different behaviors expressed as exponential functions of the electric field and/ or temperature. The maximum dielectric strength was found to be in the order of 10^7 V/cm.

Noskov et al. investigated the thermal instabilities initiated by a local temperature disturbance using numerical modelling [5]. They used a model based on a system of three coupled equations, i.e., electric potential, charge density and temperature, to study the development of the dielectric thermal breakdown. They performed these studies for polyimide insulation. Using three different time constants, i.e., Maxwell charge relaxation time, temperature disturbance dissipation time, and conductivity rise time, they characterized the different possibilities of thermal instabilities and breakdown: homogeneous heating, heating of a local region inside the dielectric, and current constriction and heating of a channel between the electrodes.

Although extensive studies have been made regarding the dielectric breakdown on conductive and semiconductive solids and polymeric insulators, a remarkably low number of studies have been done regarding the thermal dielectric breakdown of wood. Additionally, the study of breakdown has been done from the perspective of electric insulators; thus, the main objective is to prevent it from happening.

Our objective in contrast, focuses on the understanding of the development of thermal breakdown so that we can induce it. The purpose of inducing thermal dielectric breakdown is to use it as a starting point for pyrolysis and biomass gasification. In this paper we study the behavior of thermal instabilities leading to thermal dielectric breakdown using a two-dimensional finite difference model.

NOMENCLATURE

A	[$(\Omega \cdot m)^{-1}$]	Constant
B	[K^{-1}]	Constant
C_V	[$J/m^3 \cdot K$]	Specific heat at constant volume
E	[V/m]	Electric field
f	[Hz]	Frequency
j	[A/cm^2]	Current density
k	[W/m·K]	Thermal conductivity
L	[m]	Domain length
t	[s]	Time
$\tan(\delta)$	[-]	Loss tangent
T	[K]	Absolute temperature
T_c	[K]	Critical temperature
T_p	[K]	Pyrolysis temperature
T_0	[K]	Initial temperature

Greek Symbols

ε	[-]	Dielectric constant
γ	[$(\Omega \cdot m)^{-1}$]	Electrical conductivity
ω	[rad/s]	Frequency
ϕ_0	[V]	Applied electric potential
ϕ	[V]	Electric potential

Subscripts

y	[-]	y-direction

NUMERICAL MODEL

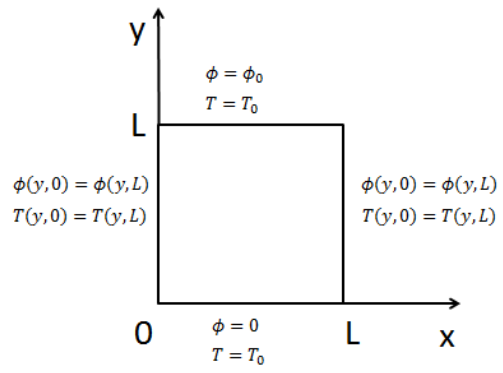

Figure 1 Computational Domain.

Computational Domain

A two dimensional computational domain of size $L \times L$ in both x and y directions is used, as shown in Fig. 1. The domain was divided into 50×50 divisions with a length L of 0.01 m and a time step of 0.01 seconds. Both grid independence and time

independence tests were performed to obtain the above grid size and time step. Results for the middle temperature for case 1 are shown in Table 2.

Table 1 Grid independence test using case 1: T_0=300 K, ϕ_0=2000 V, final time 8 seconds.

Number of grids	Middle temperature T(x=0.5 cm, y=0.5 cm), [K]	Absolute relative error [K]
20	397.6236	-
40	397.6530	0.0294
50	397.6565	0.0035
60	397.6583	0.0018
80	397.6602	0.0019

Mathematical Equations

The following model is used for the study of dielectric thermal breakdown of wood, where the charge density is assumed constant [7]:

$$0 = \nabla \cdot (\gamma \nabla \phi) \tag{2}$$

$$C_v \frac{\partial T}{\partial t} = \nabla \cdot (k \nabla T) + \gamma \cdot (\nabla \phi)^2 \tag{3}$$

where γ [$(\Omega \cdot m)^{-1}$] is the electrical conductivity of wood, ϕ [V] is the electric potential, C_v [J/(m^3·K)] is the heat capacity for wood, k [W/(m·K)] is the thermal conductivity, and T is the temperature in Kelvin. While k and C_v are assumed to be constant with temperature, the DC electrical conductivity γ depends on temperature as follows [10]:

$$\gamma(T) = Ae^{BT} \tag{4}$$

where $A = 2 \cdot 10^{-13}$ [$(\Omega \cdot m)^{-1}$] and $B = 0.0693$ [K^{-1}]. The current density in the *y*-direction is given as [7]:

$$j_y = -\gamma \frac{\partial \phi}{\partial y} \tag{5}$$

Initial and Boundary Conditions

The initial and boundary conditions for the heat equation and the electric potential equation are described in Table 2.

Numerical methods

The alternating direction implicit (ADI) algorithm was employed to solve the 2D coupled equations [11]. The tri-diagonal matrix algorithm (TDMA) was used to solve the resulting tri-diagonal systems of equations. The code was implemented in MATLAB®.

The following values were used for wood for all the simulations. The thermal conductivity and specific heat capacity are evaluated at the initial temperature with the following values, 0.12 W/m·K and $0.35 \cdot 10^3$ J/m^3·K, respectively [10]. The electrical conductivity is also evaluated at T_0, but it changes with temperature accordingly. The simulations are run for a specified time or until pyrolysis temperature of approximately T_p=750 K is reached.

Table 2 Initial and boundary conditions.

Case #	Initial Conditions, Temperature	Boundary Conditions, Temperature	Boundary Conditions, Electric Potential
1	$T(0,x,y) = T_0$	Constant $T(t,x,0) = T_0$ $T(t,x,L) = T_0$ Periodic $T(0,y) = T(L,y)$	Constant $\phi(x,L) = \phi_0$ $\phi(x,0) = 0$ Periodic $\phi(0,y) = \phi(L,y)$
2			
3		Constant $T(t,x,0) = T_0$ $T(t,x,L) = T_0$ Constant $T(t,0,y) = T_0$ $T(t,L,y) = T_0$	
4		Constant $T(t,x,0) = T_0$ $T(t,x,L) = T_0$ Periodic $T(0,y) = T(L,y)$	
5			

RESULTS AND DISCUSSION

The two-dimensional model was used to study the thermal instabilities leading to thermal dielectric breakdown of biomass. The breakdown process was analyzed for several cases described in Table 3. In case 1, γ was kept constant at its initial value at T_0=300 K. Periodic boundary conditions were used at $x = 0, L$ for both electric potential and temperature. Figure 2 shows a contour temperature distribution at $t = 8$ seconds, and Fig. 3 shows the two-dimensional temperature distribution at $x = 0.5$ cm. The maximum temperature reached was near 400 K. Note that only one *x* location is plotted for this and most other cases in subsequent figures, for given the periodic boundary conditions on the east and west sides, most curves overlap.

Table 3 Matrix of cases ran.

Case #	Electrical conductivity, [$(\Omega \cdot m)^{-1}$]	T_0, [K]	Electric Potential (DC) ϕ_0, [V]	Frequency, [Hz]	Maximum time, [s]
1	γ =constant	300	2000	-	8
2	$\gamma(T)$			-	1.17
3				-	
4			2000, 4000, 6000	-	
5	$\gamma(T,f)$	400	4000 (AC)	20, 100, 10k	6

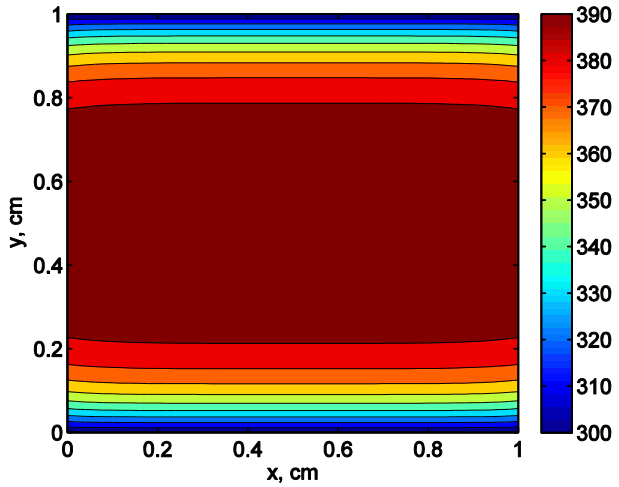

Figure 2 Contour of the temperature distribution at t=8 seconds; case 1: γ=constant, ϕ_0=2000 V, T_0=300 K.

Figure 4 shows the electric potential variation with y at $x = 0.5$ cm. The electric potential varies linearly with y because the electrical conductivity γ is independent of temperature. The current density stays constant at $4.276 \cdot 10^{-3}$ A/cm^2, and, therefore it is not plotted.

Figure 5 shows the change in temperature over time at $x = 0.5$ cm and three distinct y locations, i.e. y = 0.04, 0.1, and 0.5 cm, respectively. It is seen that the temperature increases steadily at all three locations with a higher slope at y = 0.5cm

For case 2, the conditions are the same as for case 1, but with the electrical conductivity as a function of temperature as specified by eq. 4. Figure 6 shows the temperature variation with y at $x = 0.5$ cm and at a time t=1.17 seconds. It can be seen from the figure that the temperature slopes at $y = 0, L$ are much steeper than for case 1.

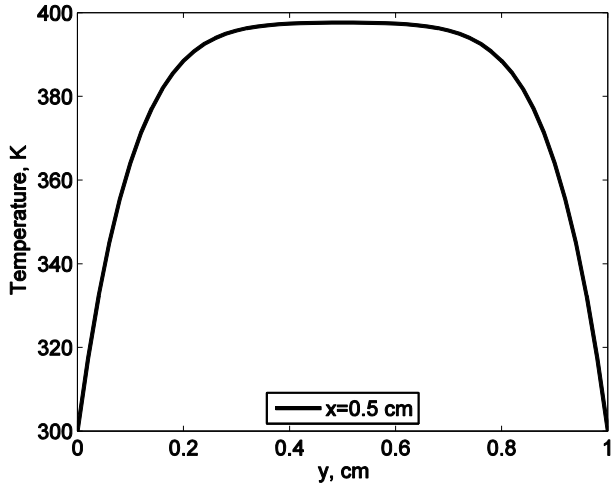

Figure 3 Temperature variation with y at $\boldsymbol{x = 0.5}$ cm and at time t=8 seconds; case 1: γ=constant, ϕ_0=2000 V, T_0=300 K.

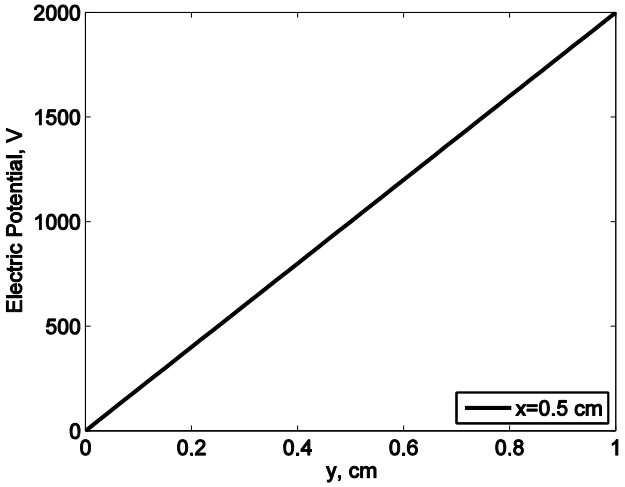

Figure 4 Electric potential variation with y at $\boldsymbol{x = 0.5}$ cm at time t=8 seconds; case 1: γ=constant, ϕ_0=2000 V, T_0=300 K.

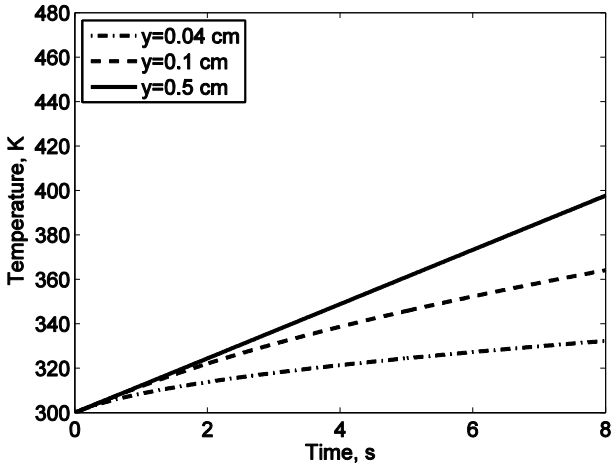

Figure 5 Temperature vs time at $\boldsymbol{x = 0.5}$ cm and three different y locations; case 1: γ=constant, ϕ_0=2000 V, T_0=300 K.

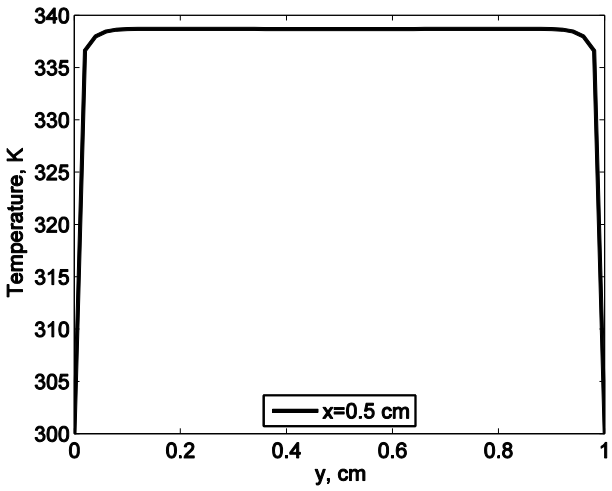

Figure 6 Temperature variation with y at $\boldsymbol{x = 0.5}$ cm and at time t=1.17 seconds; case 2: $\gamma = \gamma(T)$, ϕ_0=2000 V, T_0=300 K.

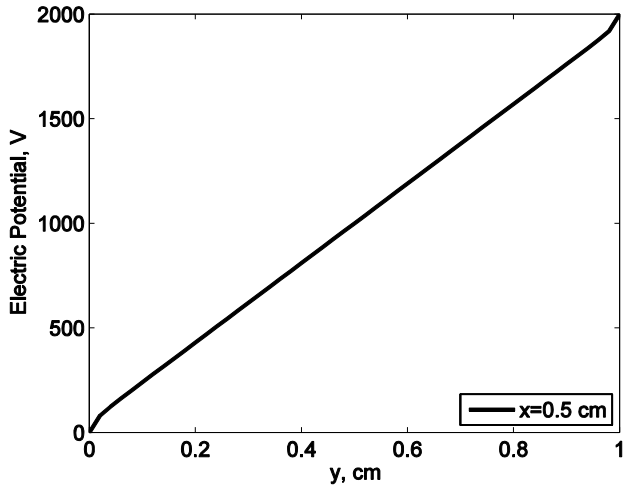

Figure 7 Electric potential variation with y at $x = 0.5$ cm and at time t=1.17; case 2: $\gamma = \gamma(T)$, ϕ_0=2000 V, T_0=300 K.

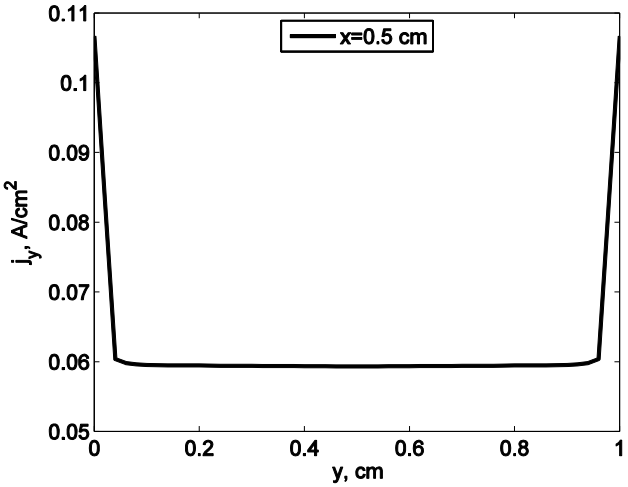

Figure 8 Current density variation with y at $\boldsymbol{x = 0.5}$ cm and at t=1.17 seconds; case 2: $\gamma = \gamma(T)$, ϕ_0=2000 V, T_0=300 K.

The second feature differing from case 1 is the electric potential. Figure 7 shows how the electric potential variation with y has changed from the perfectly linear profile to a steep curvature at the $y = 0, L$ boundaries. Thirdly, Fig. 8 shows an overall higher current distribution than case 1, and higher currents can be seen at the edges due to the high potential gradient at the boundaries. This is about 1 order of magnitude higher than in case 1. Lastly, Fig. 9 shows the rapid increase of temperature with time after one second. These conditions are indicative of reaching breakdown quickly. Two curves were plotted for temperature corresponding to two points in the domain, one near the edge at $y = 0.04$ cm and $x = 0.5$ cm and another one at the center $x = y = 0.5$ cm.

Case 3 was run using constant temperature boundary conditions in all four sides, while the rest of the operating conditions were the same as for case 2. The contour temperature distribution is shown in Fig. 10. The temperature slope is much higher at the $y = 0, L$ boundaries where the electrodes are placed indicating a much faster change in conductivity close to these boundaries.

Case 4 was run for three different electric potentials while the rest of the operating conditions were kept the same as in case 2. Figure 11 shows the temperature development over time at the center point of the domain x=y=0.5 cm. It can be readily seen that as the electric potential is increased, the temperature rises much more quickly leading to almost instantaneous thermal breakdown. Similar results can be achieved if the length is decreased while the voltage is kept constant.

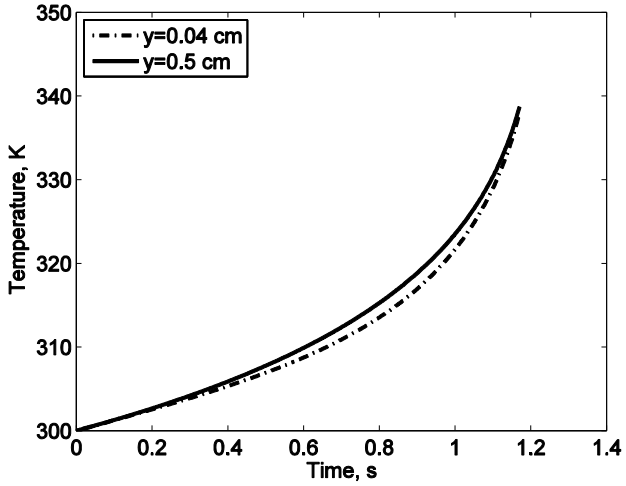

Figure 9 Temperature vs time; case 2: $\gamma = \gamma(T)$, ϕ_0=2000 V, T_0=300 K. The shown temperatures correspond to two points in the domain with the shown coordinates in y and $\boldsymbol{x = 0.5}$ cm.

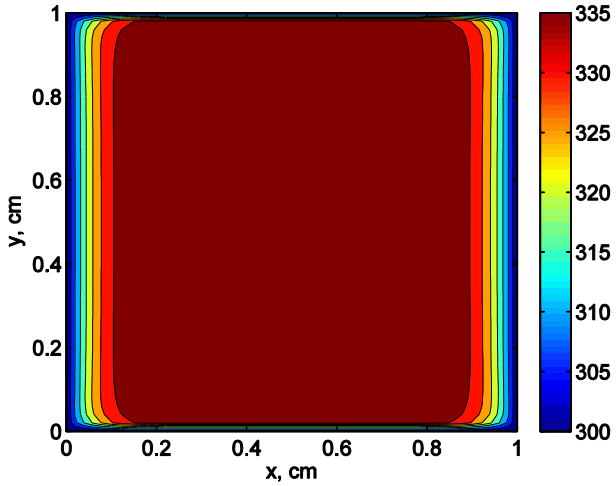

Figure 10 Temperature distribution; case 3: $\gamma = \gamma(T)$, ϕ_0=2000 V, T_0=300 K, and constant temperature boundary conditions at all four walls.

AC conductivity

While all the previous cases were run utilizing the DC voltage and conductivity of wood, case 5 analyzes the dielectric breakdown process under AC voltage at three different frequencies. For a specified temperature and moisture content, the AC conductivity is expressed as [12]:

$$\gamma = \omega \cdot \varepsilon \cdot \tan\delta \qquad (6)$$

where, ω [rad/s] is the frequency, ε is the dielectric constant, and $\tan\delta$ is the loss tangent. The electrical conductivity dependence on temperature is also exponential [13], and varies nonlinearly with frequency and moisture content [12,13].

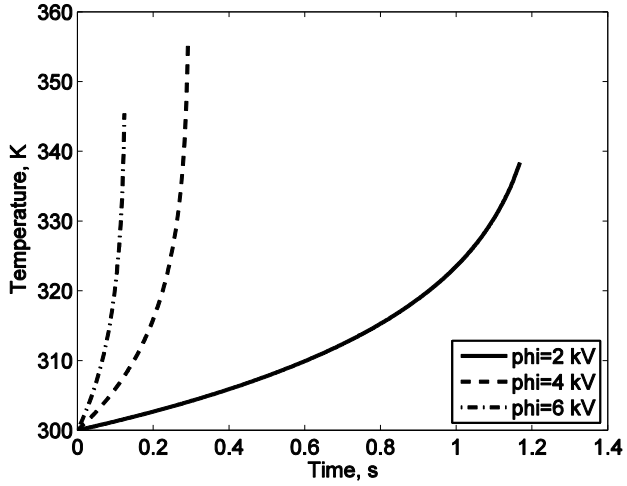

Figure 11 Temperature vs time; case 4: $\gamma = \gamma(T)$, ϕ_0=2000, 4000, 6000 V, T_0=300 K. The shown temperatures correspond to the center of the domain x=y=0.5 cm.

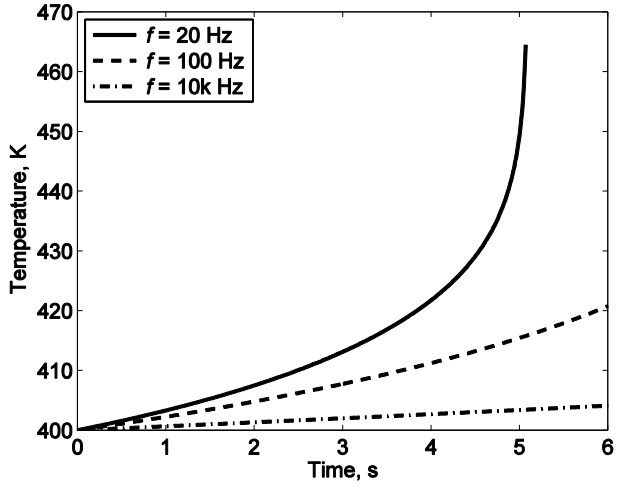

Figure 12 Temperature vs time; case 5: $\gamma = \gamma(T,f)$, ϕ_0=4000 V (AC), T_0=400 K. f=20, 100, 10k Hz, The shown temperatures correspond to the center of the domain x=y=0.5 cm.

The results in Fig. 12 show the temperature development over time for the three frequencies. It can be seen that, as opposed to voltage, when the frequency is decreased the temperature rises much more quickly, leading to breakdown much sooner. It is worth mentioning that for lower temperatures, the opposite trend is true, higher frequencies lead to breakdown more quickly, since at lower temperatures the conductivity increases with frequency. Also it is noted that the initial temperature in this case is $T_0 = 400$ K.

These overall results suggest that breakdown conditions can be achieved even when no local defects or weak-points are assumed and starting with a uniform temperature distribution. Based on these results we can infer that high electric potential or equivalently, higher electric fields, lead to almost instantaneous thermal dielectric breakdown. This in turn shows that breakdown induced by high electric fields can be used as an efficient method for biomass gasification since the heat is released directly inside the biomass. This system may reach higher efficiencies compared to conventional downdraft gasifiers [1], where a fraction of energy is used to heat up the incoming biomass, and plasma assisted gasifiers [2,3] , where also a fraction of energy is lost into the surroundings before it reaches the biomass.

CONCLUSIONS

A two-dimensional finite difference model was developed to study the thermal dielectric breakdown of biomass. Results showed that a temperature dependent electrical conductivity causes the bulk temperature to increase more quickly leading to almost instantaneous breakdown conditions. It was shown that thermal instabilities are caused by the temperature dependent electrical conductivity even when no local defects or weak-points are found in the biomass.

Temperature increased faster for higher voltages for the DC conductivity and for lower frequencies for the AC conductivity. These results, thus, suggest that high electric potential or thin pieces of biomass are desired for sustainable gasification purposes.

REFERENCES

[1] Garcia-Bacaicoa, P., Mastral, J., Ceamanos, J., Berrueco, C., and Serrano, S., Gasification of biomass/high density polyethy-lene mixtures in a downdraft gasifier, *Bioresource technology,* Vol. 99, No. 13, 2008, pp. 5485–5491.

[2] Hrabovsky, M., Konrad, M., Kopecky, V., Hlina, M., Kavka, T., Chumak, O., Van Oost, G., Beeckman, E., and Defoort, B., Pyrolysis of wood in arc plasma for syngas production, *High Temperature Material Processes (An International Quarterly of High-Technology Plasma Processes),* Vol. 10, No. 4, 2006.

[3] Shie, J.-L., Tsou, F.-J., Lin, K.-L., and Chang, C.-Y., Bioenergy and products from thermal pyrolysis of rice straw using plasma torch, *Bioresource technology,* Vol. 101, No. 2, 2010, pp. 761–768.

[4] O'Dwyer, J. J., Theory of dielectric breakdown in solids, *Journal of The Electrochemical Society,* Vol. 116, No. 2, 1969, pp. 239–242.

[5] Noskov, M., Cheglokov, A., and Shapovalov, A., Dynamics of the thermal instability evolution in dielectric breakdown, *Russian Physics Journal,* Vol. 44, No. 1, 2001, pp. 48–54.

[6] Nagao, M., Kitamura, T., Mizuno, Y., Kosaki, M., and Ieda, M., Localized heat generation before dielectric breakdown of polyethylene films. *In Conduction and Breakdown in Solid Dielectrics, Proceedings of the 3rd International Conference on,*

IEEE, 1989, pp. 77–81.
[7] O'Dwyer, J. J., *The theory of electrical conduction and breakdown in solid dielectrics*, Clarendon Press Oxford, 1973.
[8] Frolich, H., On the theory of dielectric breakdown in solids, *Proceedings of the Royal Society A,* Vol. 188, No. 1015, February, 1947, 521–532.
[9] Sze, S., Current transport and maximum dielectric strength of silicon nitride films, *Journal of Applied Physics,* Vol. 38, No. 7, 1967, 2951–2956.
[10] Simpson, W., and TenWolde, A., Wood handbook: Wood as an engineering material. *Gen. Tech. Rep. FLP-GTR-113, USDA–Forest Service, Forest Products Laboratory, Madison, WI*, 1999.
[11] Ismail, I., and Allan, M., A designed adi software for solving poisson's equation, *MATHEMATICAL AND COMPUTA-TIONAL APPLICATIONS,* Vol. 9, 2004, pp. 157–164.
[12] Torgovnikov, G. I., *Dielectric properties of wood and wood-based materials*, Springer Berlin Heidelberg, 1993.
[13] James, W. L., Dielectric properties of wood and hardboard: Variation with temperature, frequency, moisture content, and grain orientation, *Tech. rep., DTIC Document*, 1975.